

Erosion effects due to a hot liquid jet impinging obliquely on a solid plate

L.Castellano

Matec/Modelli Matematici S.r.l., Milano, Italy

L.Biasi

Department of Structural Mechanics, University of Pavia, Italy

A.Benuzzi & A.Yerkess

Commission of the European Communities, Joint Research Centre, Ispra Establishment, Italy

1 INTRODUCTION

One of the scenarios to be considered in the safety analyses of liquid metal fast breeder reactors (LMFBR) is the consequence of a partial or total melt-down of the core. In particular, it is necessary to know if the molten fuel will penetrate structures such as the core catcher, the main reactor vessel, and in the extreme case, the safety vessel. The out-of-pile FARO test facility at JRC Ispra has been developed to investigate such accidents. For one set of experiments, the BLOKKER perforation tests, the erosion and possible penetration caused by a jet of liquid uranium dioxide impinging vertically onto a steel plate inclined at specific angles will be investigated. Other similar perforation experiments have been performed at KfK, Karlsruhe, but using a jet of molten iron.

Theoretical analysis of the erosion of a solid structure caused by the oblique impingement of a jet of hot liquid metal is very complex because the situation is fully 3-dimensional, two materials in two different phases are involved and the geometry of the impinged surface is continuously changing. In principle, a complete set of Navier-Stokes equations with initial and boundary conditions could be used but this would be computationally prohibitive due to stability timestep limitations imposed by the extremely thin ablated layer. Surface tension effects required at the boundary of two liquid materials are also difficult to compute. For these reasons a more simplified model was realized and this will be described in section 2.

A brief description of the perforation experiments will be given in section 3. Some computer code predictions will also be presented and compared with available experimental results.

2 THE MATHEMATICAL MODEL

The analysis is based on a simplified model where three different regions are defined, see Fig. 1:

- 1) an inviscid potential region where spreading of the jet occurs;
- 2) a viscous boundary layer mixture of liquid jet and molten structure;
- 3) the solid structure.

Depending on the temperature range, a solid crust can form between the molten structure material and the jet material.

This simplified model is based on the following hypotheses:

- region 1 is assumed irrotational because entrainment and gravity effects are negligible if the jet length is small;
- the strong acceleration in the stagnation zone ensures that the flow regime in the viscous boundary layer is laminar;
- when no stable crust exists, the molten structural material is entrained in the viscous region and completely mixes with the jet material.

The computational procedure is outlined in the following steps:

- a) the flow within region 1, the jet, is solved numerically using a finite element method (code JET3D);
- b) fluid velocities along the structure obtained in step a) are interpolated and an analytic form of the inviscid flow is obtained;
- c) the boundary layer equations with the external flow given by step b) are solved numerically (code BOUNDY). Assuming the structure to be semi-infinite and having constant thermophysical properties, this step also provides the flux applied to it;
- d) the energy equations are solved numerically (code MELT) and the melting front propagation in the real finite structure is determined.

The results from steps a) to c) are obtained under quasi steady-state conditions, whereas step d) provides a description of erosion in time. Hence, to take into account the deformation of the impinged surface due to melting and ablation, steps a) to c) can be repeated after any selected time interval.

2.1 Hydrodynamics of the potential region

With reference to Fig. 2, the equations to be solved are

$$\underline{v} = \nabla\phi \quad (1)$$

$$\nabla^2\phi = 0 \quad (2)$$

$$\nabla\phi \cdot \underline{n} = 0 \quad \text{everywhere on the free surface FS} \quad (3)$$

$$\nabla\phi \cdot \underline{n} = v_J \quad \text{everywhere on the efflux surface ES} \quad (4)$$

$$\phi = \text{const.} \quad \text{everywhere on the influx plane IP} \quad (5)$$

$$|\underline{v}| = v_J \quad \text{everywhere on the free surface FS} \quad (6)$$

where \underline{v} is the velocity vector, v_J the initial jet velocity, ϕ the potential, and \underline{n} the unit vector normal to the boundary indicated.

The numerical procedure may be summarized as follows:

- a) a first guess of the location of the free surface is made;
- b) solve Eqs.(2) to (5) in the domain bounded by the free surface;
- c) the local velocities on the free surface are evaluated using (1);
- d) an adjustment to the position of the free stream-lines proportional to the value of the difference

$$\left(\frac{|\underline{v}|}{v_J} \right)^2 - 1 = \epsilon \quad (7)$$

is locally performed;

- e) the steps b) to d) are repeated until the condition

$$\left| \frac{|\underline{v}|}{v_J} - 1 \right| < \epsilon_0 \quad (8)$$

is satisfied.

2.2 Thermo-hydrodynamic equations for the viscous boundary layer

The velocity components (u_ℓ, v_ℓ, w_ℓ) on the lower boundary of region 1 in the neighbourhood of the stagnation point can be represented as a power series truncated to the second order (Lesin, 1976)

$$u_\ell = ax + cx^2; \quad v_\ell = ay; \quad w_\ell = -2ax - 2cxz \quad (10)$$

where the constants a and c are computed from the potential solution along the common surface between the jet and the plate, the coordinate axes being indicated in Fig. 2. Velocities and coordinates are made dimensionless using the jet velocity V_J , and jet diameter D_J , respectively.

In the boundary layer near the stagnation point, the corresponding velocity components can be written in the following form

$$\begin{aligned} u &= ax\phi'(\eta) + cx^2\xi'(\eta) \\ v &= ay\phi'(\eta) \\ w &= -2\sqrt{\frac{a}{\text{Re}}}\phi(\eta) - 2\frac{cx}{\sqrt{a\text{Re}}}\xi(\eta) \end{aligned} \quad (11)$$

where $\eta = \sqrt{a\text{Re}}.z$; $\text{Re} = \rho V_J D_J / \mu$; ρ is the jet density and μ is the jet dynamic viscosity.

Assuming there is no stable crust formation between the jet and plate, the temperature is represented by the expression

$$T = T_{\text{ms}} + (T_J - T_{\text{ms}})(\theta_1(\eta) + \frac{2cx}{a} \cdot \theta_2(\eta)) \quad (12)$$

where T_J is the jet temperature and T_{ms} is the plate melting temperature. Substituting expressions (11) and (12) into the boundary layer equations, the following system of ordinary differential equations is obtained

$$\phi''' + 2\phi\phi'' - \phi'^2 + 1 = 0 \quad (13)$$

$$\xi''' + 2\phi\xi'' - 3\phi'\xi' + 2\phi''\xi + 3 = 0 \quad (14)$$

$$\theta_1'' + 2\text{Pr}\phi\theta_1' = 0 \quad (15)$$

$$\theta_2'' + 2\text{Pr}\phi\theta_2' - \text{Pr}\phi'\theta_2 + \text{Pr}\xi\theta_1' = 0 \quad (16)$$

where Pr is the Prandtl number.

The boundary conditions associated with Eqs.(13)-(16) are

$$\begin{aligned} \phi'(0) &= \xi'(0) = \theta_1(0) = \theta_2(0) = 0 \\ -2\sqrt{\frac{a}{\text{Re}}}\phi(0) - 2\frac{cx}{\sqrt{a\text{Re}}}\xi(0) &= w_0 \\ \phi'(\infty) &= \xi'(\infty) = \theta_1(\infty) = 1 \\ \theta_2(\infty) &= 0 \end{aligned} \quad (17)$$

where w_0 is the velocity of the material coming into the boundary layer

from the melting plate and is obtained from Eq.(18) assuming:
- the plate is semi-infinite in the z-direction;
- the plate physical properties do not vary with temperature;
- the geometry is locally one-dimensional and quasi steady-state;

$$w_o = \frac{k\sqrt{aRe}}{\rho D_J V_J} \frac{T_J - T_{ms}}{L + c_s(T_{ms} - T_{in})} (\theta'_1(0) + \frac{2cx}{a} \theta'_2(0)) \quad (18)$$

where k , ρ , L , c_s , T_{in} are thermal conductivity, density, latent heat, specific heat and initial temperature of the metal plate, respectively.

The heat flux applied to the structure in the region of the stagnation point can be computed using the expression

$$k \left. \frac{\partial T}{\partial z} \right|_o = \frac{k\sqrt{aRe}}{D_J} (T_J - T_{ms}) (\theta'_1(0) + \frac{2cx}{a} \theta'_2(0)) \quad (19)$$

To determine the heat flux outside the stagnation region, an integral method adapted by Lipsett-Gilpin (1978) is employed thus obtaining the expression

$$k \left. \frac{\partial T}{\partial z} \right|_o = \frac{2\Delta}{1 + \gamma Pr} \frac{k\sqrt{Re}(T_J - T_{ms})}{D_J \sqrt{2\Delta} \left[\frac{2}{Pr(1 + \gamma Pr)} + 6\gamma \right] \frac{x}{D_J} + b} \quad (20)$$

where Δ is the dimensionless thickness of the layer and γ is given by the expression

$$\gamma = \frac{\sqrt{1 + 4Ste} - 1}{2Pr} \quad \text{where } Ste = \frac{c_s(T_J - T_{ms})}{L + c_s(T_{ms} - T_{in})}$$

The constant b in Eq.(20) is determined in such a way that the two expressions become equal at the boundary of the stagnation region.

2.3 Melting of the structure

To determine the melting front propagation in the plate, the energy equation is solved using a body-fitted coordinates method (Thompson et al., 1974), which has the advantage of performing computations on a fixed rectangular grid. The energy equation in the transformed plane (η, ξ) is written

$$\begin{aligned} T_t = \alpha_s \left[\frac{1}{J^2} (\gamma_{11} T_{\xi\xi} + \gamma_{22} T_{\eta\eta} + 2\gamma_{12} T_{\xi\eta}) + P T_{\xi} + Q T_{\eta} \right] \\ + \alpha_s \frac{d \ln k}{dT} \frac{1}{J^2} \left[(z_{\eta} T_{\xi} - z_{\xi} T_{\eta})^2 + (x_{\xi} T_{\eta} - x_{\eta} T_{\xi})^2 \right] \\ + \frac{1}{J} \left[(z_{\eta} T_{\xi} - z_{\xi} T_{\eta}) x_t + (x_{\xi} T_{\eta} - x_{\eta} T_{\xi}) z_t \right] \end{aligned} \quad (21)$$

where J is the Jacobian transform and α_s and k_s are the plate diffusivity and conductivity, respectively. P and Q are the functions which control the spacings between the grid lines (Thomas & Middlecoff, 1980).

$$\left. \begin{aligned} P(\xi, \eta) &= -(\dot{x}_\xi \dot{x}_{\xi\xi} + z_\xi z_{\xi\xi}) / (\dot{x}_\xi^2 + z_\xi^2) (\xi_x^2 + \xi_z^2) \\ Q(\xi, \eta) &= -(\dot{x}_\eta \dot{x}_{\eta\eta} + z_\eta z_{\eta\eta}) / (\dot{x}_\eta^2 + z_\eta^2) (\eta_x^2 + \eta_z^2) \end{aligned} \right\}$$

The melting front propagation is described by the boundary condition

$$x_t = (q_x + \frac{k_s}{J} z_\xi T_\eta) / \rho_s L; \quad z_t = (q_z - \frac{k_s}{J} x_\xi T_\eta) / \rho_s L \quad (23)$$

where q_x and q_z are the heat flux components corresponding to the x and z directions, respectively, as defined in Eqs. (19) and (20).

3 PREDICTIONS FOR THE KfK EXPERIMENTS

KfK has performed a series of perforation experiments (Jochim et al.) in which a jet of molten iron falls onto a stainless steel plate which can be inclined at various angles, see the schematic illustration in Fig. 3. 100 kg of thermite powder are ignited in a specially designed reaction crucible. Some seconds after the completed reaction two distinct strata are formed, the lower layer contains about 55 kg of pure iron and the upper layer contains a mixture of the oxides of aluminium, iron and magnesium.

A rupturing of the seal at the base of the reaction crucible allows the melt to fall freely after passing through an orifice of known diameter. Until a uniform jet flow is established the melt falls onto a deflector tube which guides it into a magnesium oxide receptacle containing sand. Moving the deflector tube quickly out of the path of the jet allows it to impinge directly onto the steel specimen under test.

During the KfK investigations, several experiments were performed. In one experiment, presented here, the mean velocity and diameter of the jet were predicted to be 5.3 m/s and 12.8 mm, respectively, as it impinged onto a 4 cm thick stainless steel plate specimen inclined at an angle of 45 degrees to the vertical axis of the jet. Pyrometer measurements of the molten iron jet during free fall revealed that its temperature was approximately 2223 K. Although the time required to release the whole thermite melt was about 50 s, in fact the specimen was perforated in only 3 sec.

In Fig. 4 is seen a cross-section of the jet model which impinges the plate at 45°, there being 140 20-node 3-D solid elements in the whole mesh. From the solution of this potential problem the constants a and c in Eq. (11) were derived ($a=1.3$, $c=-0.5$) and fed into the code BOUNDY with the appropriate temperature data and physical constants in order to derive the heat flux relationships to be used by the code MELT. The program MELT cannot handle a plate perforation and for this reason the numerical mesh was extended to a depth of 4.5 cm. In this way a reasonable perforation time can be estimated by examining when the melting front reaches the depth of 4 cm.

Using the above mentioned experimental data, and assuming that the vertical heat flux distribution remains constant, the code predicts the plate penetration time to be 2.24 sec. In Fig. 5 one can see the melting line propagation in the x - z plane every 0.2 sec up to 2.2 sec, and in Fig. 6 a complete mesh configuration at 2.2 sec is shown. Of course, it must be noted that this is the time for the initial penetration, further time would be required to establish a hole of sufficient size to be detected experimentally.

The predicted penetration time calculated by the code MELT is basically a function of the normal heat flux applied to the upper surface of the plate specimen. On the other hand, the heat flux supplied by the code BOUNDY is a function of the jet characteristics, that is its velocity, diameter and temperature. In order to examine the heat flux variations due to uncertainties in these quantities, further BOUNDY calculations were executed. The jet velocity was varied from 4.3 to 6.3 mm, the jet diameter was varied from 11.5 to 14.1 mm, and finally the jet temperature was varied from 2123 to 2323 K. The heat flux distributions for these three sets of calculations are shown in Figs. 7, 8 and 9, respectively. It can be seen that the heat flux distributions are more sensitive to variations in the jet temperature. MELT calculations for the three temperatures were executed and Fig. 10 shows how the penetration time varies as a function of temperature.

4 CONCLUSIONS

Considering all the simplified assumptions and numerical steps made during the use of the codes JET3D, BOUNDY and MELT, the final result is in good agreement with experiment. It remains to be seen if the agreement will also be good for other KfK experiments in which the angle of impingement is different. As the original scope of using the codes was to predict results for the BLOKKER perforation tests, it will be interesting to make comparisons when results become available, since crust formation could play a more important role than in the KfK experiments using a thermite mixture.

REFERENCES

- Lesin, A.B. 1976. Laminar^o heat transfer near an asymmetric stagnation point, *J. of Fluid Dynamics*, 11, 940.
- Lipsett, A.W. & R.R. Gilpin 1978. Laminar jet impingement heat transfer including the effect of melting, *Int. J. of Heat and Mass Transfer*, 21, 25.
- Thompson, J.F. et al. 1974. Automatic numerical generation of body-fitted coordinate systems for fields containing any number of arbitrary two-dimensional bodies, *J. of Comput. Phys.*, 15, 299.
- Thomas, P.D. & J.F. Middlecoff 1980. Direct control of the grid point distribution in meshes generated by elliptic equations, *AIAA J.*, 18, 652.
- Jochim, H. et al. Experimente zur Wanderosion durch Schmelzstrahlen, Kernforschungszentrum Karlsruhe, private communication.

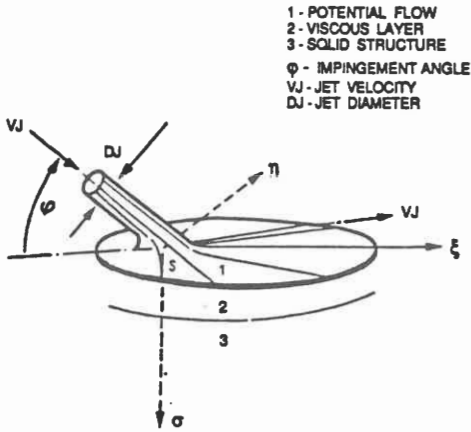


Fig. 1. Schematic diagram of the jet.

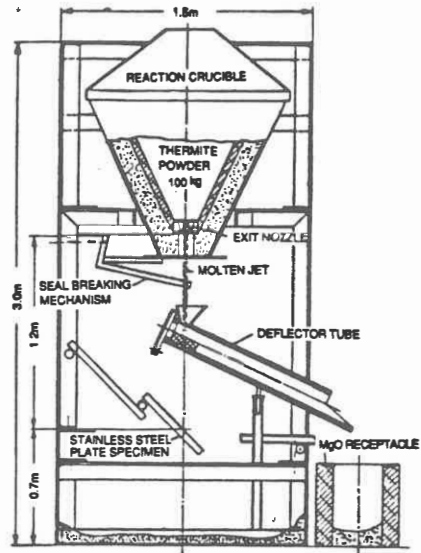


Fig. 3. The KfK penetration experiment.

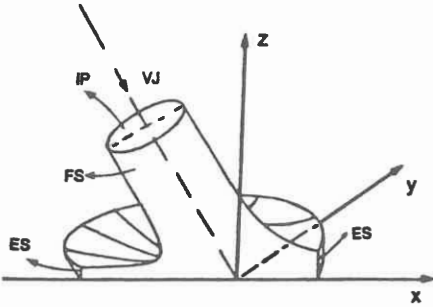


Fig. 2. Solution of the potential region.

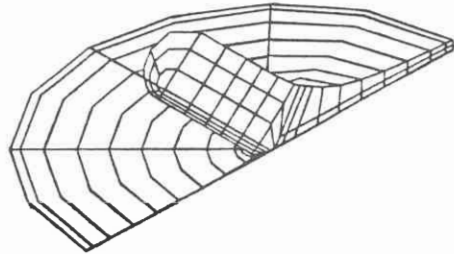


Fig. 4. Mesh discretization of the jet.

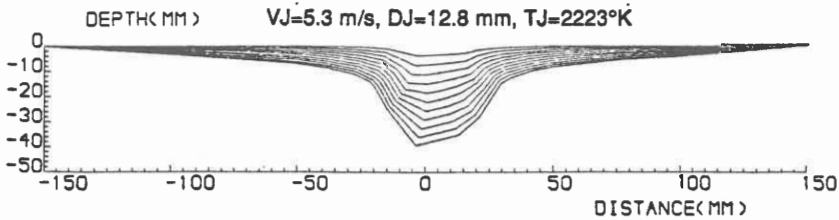


Fig. 5. Melting line propagation up to 2.2 s.

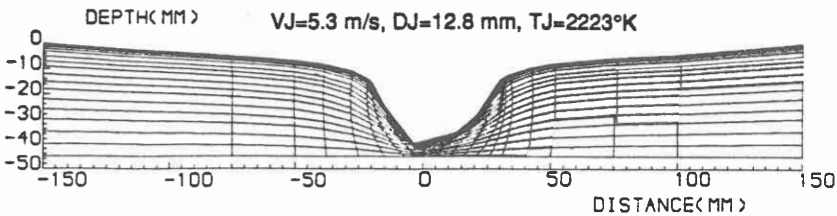


Fig. 6. Mesh configuration at 2.2 s.

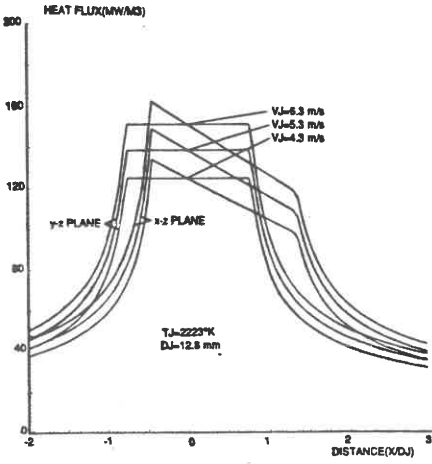


Fig. 7. Heat flux-jet velocity variations.

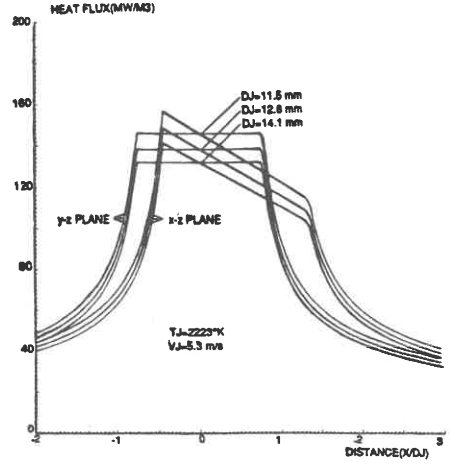


Fig. 8. Heat flux-jet diameter variations.

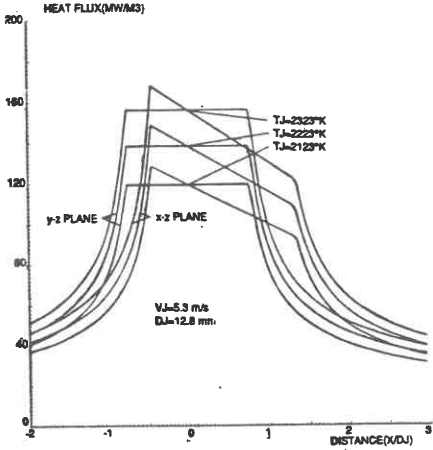


Fig. 9. Heat flux-jet temperature variations.

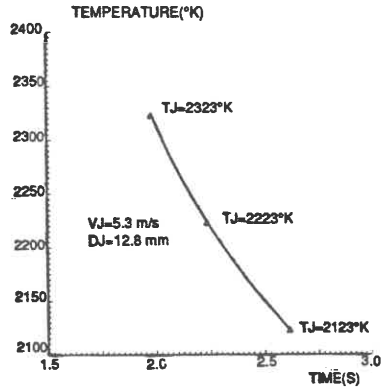


Fig. 10. Jet temperature versus perforation time.